$S_{XX}(Q)$, where H corresponds to the labelled hydrogen and X corresponds to the remaining unlabelled atoms for each set of three solutions.

Structure refinement

The nine composite partial structure factors which resulted from analysis of the diffraction data were used as constraints in an empirical potential structure refinement (EPSR)[23–25] simulation of the mixture, fixed at the experimental density and temperature. The cubic simulation box of side 26.77 Å contained 245 methanol and 105 water molecules. The seed potentials for the simulation were taken from the literature[15]. The EPSR procedure modifies these starting potential energy functions so as to make the simulated structure factors match as closely as possible the measured functions. An example of some of the fits is shown in Fig. 1. This leads to an ensemble of model molecular distributions that are consistent with the measured diffraction data.

Structure analysis

From these molecular assemblies, ensemble-averaged site–site radial distribution functions (RDFs), $g_{\alpha\beta}(r)$, can be estimated, as can other structural quantities as described below, all of which are consistent with the experimental data. Near-neighbour coordination numbers are estimated from these RDFs by integration: $N_{\alpha\beta} = 4\pi\rho_\beta \int_{r_{min}}^{r_{max}} g_{\alpha\beta}(r) r^2 \, dr$, where $N_{\alpha\beta}$ is the coordination number of β atoms around α atoms, ρ_β is the number density of β atoms in the liquid, and the range of integration is normally chosen to coincide with minima in the respective RDF. Uncertainties in these values are estimated from the observed fluctuations of $g_{\alpha\beta}(r)$ in the course of the simulation.

Cluster analysis is achieved by considering two water molecules to belong to the same cluster if they are separated by 3.5 Å or less—this is the position of the first minimum in the O_WO_W radial distribution function. The size of a water cluster is then determined by counting all the water molecules that lie within the specified distance range of each other.

Received 26 October 2001; accepted 4 March 2002.

1. Franks, F. & Ives, D. J. G. The structural properties of alcohol–water mixtures. *Q. Rev.* **20,** 1–45 (1966).
2. Franks, F. & Desnoyers, J. E. in *Water Science Reviews* Vol. 1 (ed. Franks, F.) 171–232 (Cambridge Univ. Press, 1985).
3. Murrell, J. N. & Jenkins, A. D. *Properties of Liquids and Solutions* 2nd edn 102–106 (Wiley, Chichester, 1994).
4. Frank, H. S. & Evans, M. W. Free volume and entropy in condensed systems. III. Entropy in binary liquid mixtures; partial molal entropy in dilute solutions; structure and thermodynamics in aqueous electrolytes. *J. Chem. Phys.* **13,** 507–532 (1945).
5. Soper, A. K. & Finney, J. L. Hydration of methanol in aqueous solution. *Phys. Rev. Lett.* **71,** 4346–4349 (1993).
6. Turner, J. & Soper, A. K. The effect of apolar solutes on water structure: alcohols and tetraalkylammonium ions. *J. Chem. Phys.* **101,** 6116–6125 (1994).
7. Bowron, D. T., Soper, A. K. & Finney, J. L. Temperature dependence of the structure of a 0.06 mole fraction tertiary butanol–water solution. *J. Chem. Phys.* **114,** 6203–6219 (2001).
8. Tsai, J., Gerstein, M. & Levitt, M. Keeping the shape but changing the charges: A simulation study of urea and its iso-steric analogs. *J. Chem. Phys.* **104,** 9417–9430 (1996).
9. Dixit, S., Poon, W. C. K. & Crain, J. Hydration of methanol in aqueous solutions: a Raman spectroscopic study. *J. Phys. Condens. Matter* **12,** L323–L328 (1999).
10. Wakisaka, A., Komatsu, S. & Usui, Y. Solute–solvent and solvent–solvent interactions evaluated through clusters isolated from solutions: preferential solvation in water–alcohol mixtures. *J. Mol. Liq.* **90,** 175–184 (2001).
11. D'Angelo, M., Onori, G. & Santucci, A. Self-association of monohydric alcohols in water: compressibility and infrared absorption measurements. *J. Chem. Phys.* **100,** 3107–3113 (1994).
12. Egashira, K. & Nishi, N. Low-frequency Raman spectroscopy of ethanol–water binary solution: evidence for self-association of solute and solvent molecules. *J. Phys. Chem. B* **102,** 4054–4057 (1998).
13. Yoshida, K. & Yamaguchi, T. Low temperature Raman spectroscopy of aqueous solutions of aliphatic alcohols. *Z. Naturforsch. A* **56,** 529–536 (2001).
14. Finney, J. L., Bowron, D. T. & Soper, A. K. The structure of aqueous solutions of tertiary butanol. *J. Phys. Condens. Matter* **12,** A123–A128 (2000).
15. Ferrario, M., Haughney, M., McDonald, I. R. & Klein, M. L. Molecular dynamics simulation of aqueous mixtures: methanol, acetone and ammonia. *J. Chem. Phys.* **93,** 5156–5166 (1990).
16. Palinkas, G., Hawlicka, E. & Heinzinger, K. Molecular-dynamics simulations of water–methanol mixtures. *Chem. Phys.* **158,** 65–76 (1991).
17. Tanaka, H. & Gubbins, K. Structure and thermodynamic properties of water–methanol mixtures. *J. Chem. Phys.* **97,** 2626–2634 (1992).
18. Laaksonen, A., Kusalik, P. G. & Svishchev, I. M. Three-dimensional structure in water–methanol mixtures. *J. Phys. Chem. A* **101,** 5910–5918 (1997).
19. Yamaguchi, T., Hidaka, K. & Soper, A. K. The structure of liquid methanol revisited: a neutron diffraction experiment at −80°C and +25°C. *Mol. Phys.* **96,** 1159–1168 (1999); Erratum **97,** 603–605 (1999).
20. Soper, A. K. The radial distribution functions of water and ice from 220 K to 673 K and at pressures up to 400 MPa. *Chem. Phys.* **258,** 121–137 (2000).
21. Murthy, S. S. N. Detailed study of ice clathrate relaxation: Evidence for the existence of clathrate structures in some water–alcohol mixtures. *J. Phys. Chem. A* **103,** 7927–7937 (1999).
22. Soper, A. K. & Luzar, A. A neutron diffraction study of dimethyl sulphoxide-water mixtures. *J. Chem. Phys.* **97,** 1320–1331 (1992).
23. Soper, A. K. Empirical potential Monte Carlo simulation of fluid structure. *Chem. Phys.* **202,** 295–306 (1996).
24. Bowron, D. T., Finney, J. L. & Soper, A. K. A structural investigation of solute–solute interactions in aqueous solutions of tertiary butanol. *J. Phys. Chem. B* **102,** 3551–3563 (1998).
25. Soper, A. K. Tests of the empirical potential structure refinement method and a new method of application to neutron diffraction data on water. *Mol. Phys.* **99,** 1503–1516 (2001).

Acknowledgements

S. D. is supported by the Edinburgh Chalmers Scholarship and the ORS award. Funding from the EPSRC Liquid Network and help from D. Bowron at an early stage of the experiments are gratefully acknowledged.

Competing interests statement

The authors declare that they have no competing financial interests.

Correspondence and requests for materials should be addressed to A.K.S. (e-mail: a.k.soper@rl.ac.uk).

Rapid freshening of the deep North Atlantic Ocean over the past four decades

Bob Dickson*, Igor Yashayaev†, Jens Meincke‡, Bill Turrell§, Stephen Dye* & Juergen Holfort‡

* *Centre for Environment, Fisheries, and Aquaculture Science, Lowestoft NR33 OHT, UK*
† *Bedford Institute of Oceanography, Dartmouth, Nova Scotia B2Y 4A2, Canada*
‡ *Institut fur Meereskunde, 22529 Hamburg, Germany*
§ *Marine Laboratory, PO Box 101, Aberdeen AB11 9DB, UK*

The overflow and descent of cold, dense water from the sills of the Denmark Strait and the Faroe–Shetland channel into the North Atlantic Ocean is the principal means of ventilating the deep oceans, and is therefore a key element of the global thermohaline circulation. Most computer simulations of the ocean system in a climate with increasing atmospheric greenhouse-gas concentrations predict a weakening thermohaline circulation in the North Atlantic as the subpolar seas become fresher and warmer[1–3], and it is assumed that this signal will be transferred to the deep ocean by the two overflows. From observations it has not been possible to detect whether the ocean's overturning circulation is changing, but recent evidence suggests that the transport over the sills may be slackening[4]. Here we show, through the analysis of long hydrographic records, that the system of overflow and entrainment that ventilates the deep Atlantic has steadily changed over the past four decades. We find that these changes have already led to sustained and widespread freshening of the deep ocean.

The Labrador Sea is a critical location for the Earth's climate system. In its upper and intermediate layers, annual-to-decadal variations in the production, character and thickness of its convectively formed mode water (Labrador Sea Water, LSW) directly determine the rate of the main Atlantic gyre circulation[5]. Through its deeper layers pass all of the deep and bottom waters that collectively form and drive the abyssal limb of the Atlantic meridional overturning circulation. Around its margins pass the two main freshwater flows from the Arctic Ocean to the North Atlantic (by way of the Canadian Arctic archipelago and the East Greenland shelf) that have been implicated in model experiments with a slowdown or shutdown of the meridional overturning circulation[1–3].

Over the past 3–4 decades, the entire water column of the Labrador Sea has undergone radical change. From 1966 to 1992, the overall cooling of the water column of the Labrador Sea was equivalent to a loss of $8\,W\,m^{-2}$ continuously for 26 years. Its freshening (Fig. 1a) was equivalent to mixing-in an extra 6 m of fresh water at the sea surface[6]. As a result, the steric height (caused by

changes in the density of the water-column) in the central Labrador Sea was typically reduced by 8–10 cm. These are arguably the largest full-depth changes observed in the modern instrumental oceanographic record (see, for example, refs 7–9).

In the upper and intermediate layers of the Labrador Sea to the limit of convection (2,300 m or so), the long cooling and freshening tendency is thought to reflect the sustained if non-steady evolution of the North Atlantic Oscillation (NAO) from its most extreme negative state in the instrumental record during winters of the 1960s to its most extreme and prolonged positive state in the early 1990s[10]. This evolution brought deepening convection[11,12] and ultimately formed LSW that was fresher, colder, deeper and denser[13] than at any other time in the history of deep measurements there.

In the upper water column (about 0–2 km), these long-sustained cooling and freshening trends were halted or partly reversed in the late 1990s (see Fig. 1a, for data post-1995, at depths between 1,000 and 2,000 m). But the deep and abyssal layers of the Labrador Sea (2,300–3,300 m) show a remarkable freshening by more than −0.01 per decade over the past 3–4 decades; the beginnings of this continuing freshening were noted 20 years ago[14,15]. Beyond the

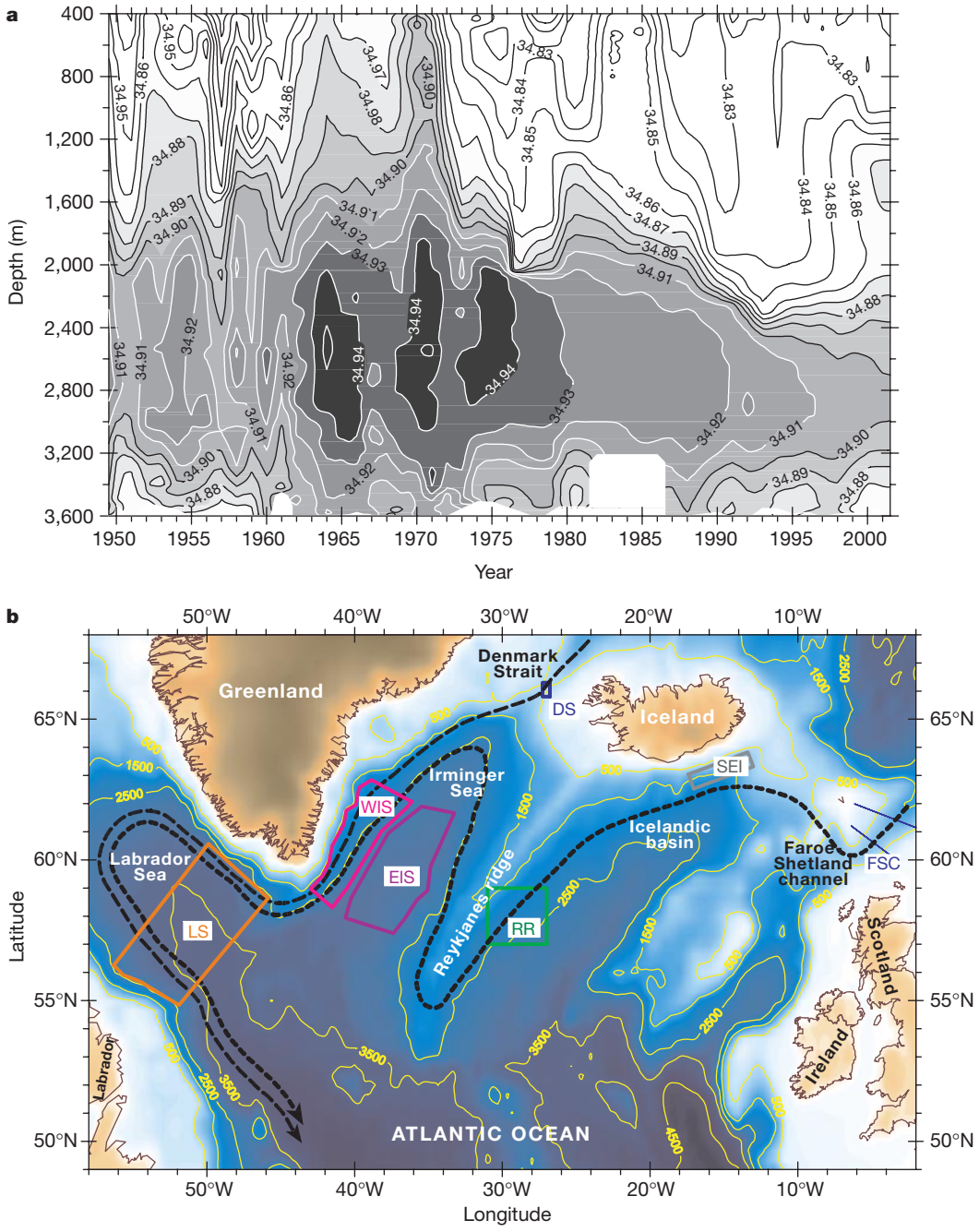

Figure 1 The origins of deep freshening in the Labrador Sea. **a**, Rapid and long-term freshening throughout the water column of the Labrador Sea. Shown are salinity changes since 1950 in the central part of the basin, with values >34.87 shaded. The data set was selected to lie within the 3,300-m isobath of the Labrador Sea, and the plot represents the median values of vertical property profiles, binned according to σ_2 density intervals. **b**, The two main overflows across the Greenland–Scotland ridge and their spreading pathways to the Labrador Sea (heavy dashed lines). Letters identify the locations of time series used in Fig. 2 to describe their changing characteristics *en route*.

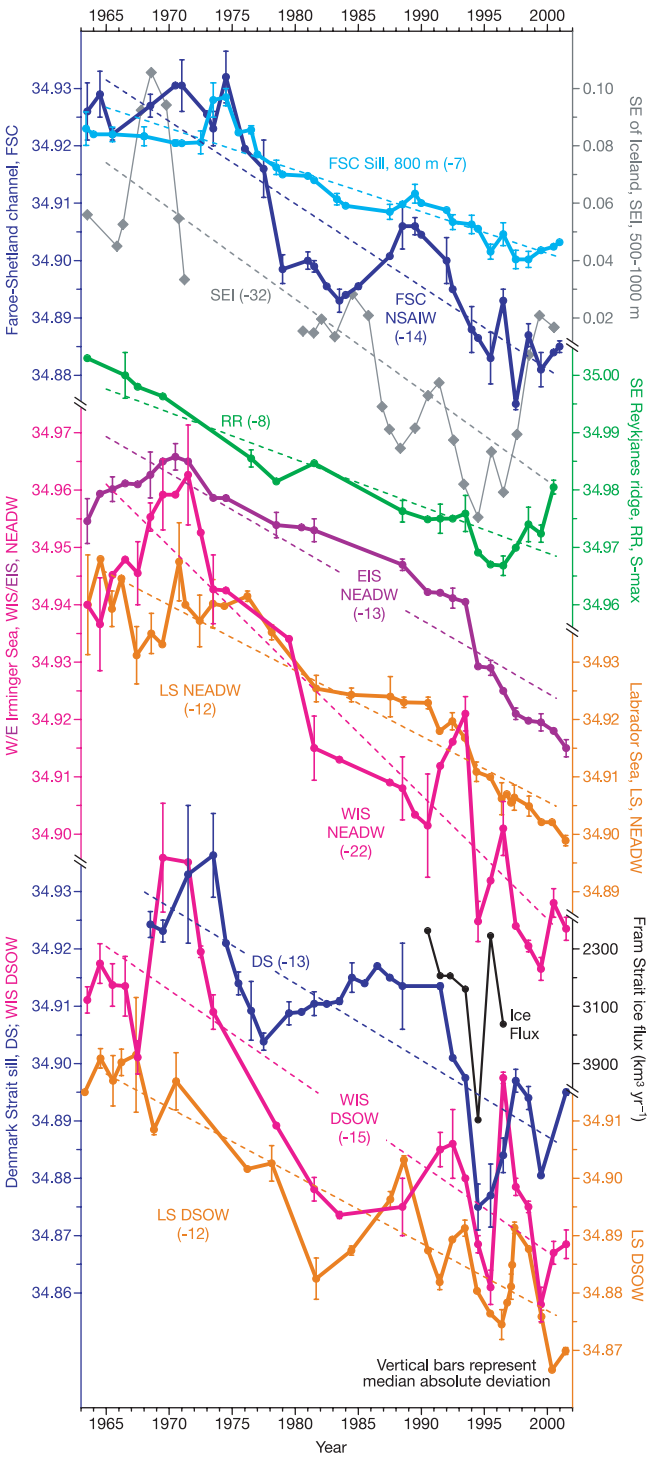

Figure 2 Evidence of sustained and rapid freshening throughout the system of overflow and entrainment that ventilates the deep Atlantic. The salinity time series shown are plotted to a common scale (with the exception of SEI at half scale), and are colour- and letter-coded to identify their locations in Fig. 1b. The mean freshening rates in p.p.m. per decade listed against each curve are calculated for the common period 1965–2000, selected as the period of the most accurate salinity data set and the period during which the North Atlantic Oscillation (NAO) exhibited a sustained change between low-index and high-index extreme states. FSC sill and FSC NSAIW describe the freshening deep outflow through the Faroe–Shetland channel at sill depth and in the Arctic Intermediate Water layer, respectively[20]. SEI shows the depth-mean anomaly of salinity in the 500–1,000 m layer at the head of the south Icelandic basin, including data from the standard Icelandic Stokksnes section, and so represents the salinity of the water masses likely to be entrained into the eastern overflow as it leaves the Faroe Bank channel. (The short-term spike of the 'great salinity anomaly' of the mid-1970s has been omitted). RR represents the product of that mixing, describing the salinity trend in the deep salinity maximum which marks the core of ISOW against the deep eastern flank of the Reykjanes Ridge at 57–59°N, 27–31°W. EIS NEADW, WIS NEADW and LS NEADW describe salinity time series at successive stages in the spreading of the eastern overflow as it continues into the Irminger Sea, shoals and alters along the Greenland slope and ultimately forms the Deep Water of the Labrador Sea. Curves DS, WIS DSOW and LS DSOW describe the salinity trends of the Denmark Strait overflow at the sill (depths of 500–550 m at $T < 0$ °C), in the 0–200 m near-bottom layer where the overflow plume descends the slope off southeast Greenland, and in the abyssal layers of the Labrador Sea, respectively. The observed annual mean ice flux through the Fram Strait, 1990–97, is shown for comparison[17] (scale inverted) as a possible remote cause of the enhanced freshening along this path in the mid-1990s.

reach of deep convection, these changes cannot be due to local climate forcing: they probably reflect variations in the two dense overflows that renew and ventilate these deepest layers, or changes in the resident water masses that are entrained as these vigorous flows descend, or both. We consider here why the overflows freshened, and why that freshening was maintained downstream.

We propose that the ultimate source of freshening of both overflows lies in a large-scale and long-term freshening of the upper 1–1.5 km of the Nordic seas, immediately upstream. That multi-decadal change has itself been attributed to a variety of causes, many of which are also associated with the amplifying NAO: an increase in the direct export of sea ice from the Arctic Ocean[16–18], an increase in precipitation along the Norwegian Atlantic Current by approximately 15 cm per winter through the extension of storm activity to the Nordic seas[18], and a range of factors internal to the Nordic seas[19]. These include an increased freshwater supply from the East Icelandic Current, a narrowing of the salty Norwegian Atlantic Current towards the coast, and a deepening of the interface between Arctic Intermediate Water and Deep Water in the Norwegian Sea[4,19].

Although we cannot yet partition the recent freshening of the Nordic seas into its contributory components, it is clear from some of our longest observational records that the change has occurred over a sufficiently deep layer (1–1.5 km) to affect the hydrographic character of both dense overflows crossing the Greenland–Scotland Ridge at sill depths of 700–900 m. Century-long hydrographic sections monitoring the outflow of upper Norwegian Sea Deep Water and Arctic Intermediate Water through the Faroe–Shetland channel (FSC sill and FSC NSAIW in Fig. 2) confirm that salinities have decreased there almost linearly by ~0.01 per decade since the mid 1970s[20], and our more gappy record from the deepest part of the Denmark Strait sill (DS in Fig. 2, representing salinities at 500–550 m depth for temperatures below 0 °C) indicates a very similar net freshening over the same period.

In addition to the change at both sills, Fig. 2 illustrates the salinity change at various intervals downstream where these overflows deepen, entrain, mix and spread, ultimately forming the deep and abyssal layers of the Labrador Sea (locations in Fig. 1b). All time series but one are to a common scale (the exception is the upper-ocean time series SEI, plotted at half-scale), and the bracketed values against each curve refer to the mean freshening rate over the common period 1965–2000. (Reflecting earlier usage (salinity defined in p.p.t.), a freshening rate of 0.014 per decade will be abbreviated here to '−14 p.p.m.').

On leaving the Faroe Bank channel, the vigorous plume of Iceland–Scotland Overflow Water (ISOW; freshening at between −7 and −14 p.p.m. per decade; Fig. 2) will broaden, slow and deepen through entrainment of 'resident' water masses at the head of the south Icelandic basin before continuing south at 1,500–2,500 m depth along the eastern flank of the Reykjanes Ridge. Constructing a salinity time series for the deep salinity maximum that marks the ISOW core in this location, we find evidence of a very similar freshening rate (RR; −9 p.p.m. per decade). The same rate, period and steadiness of freshening is maintained as the ISOW-derived layer passes at depth around the Irminger Sea (there known as North East Atlantic Deep Water, thus EIS NEADW, −13 p.p.m. per decade in Fig. 2) and into the Labrador Sea (LS NEADW, −12 p.p.m. per decade).

When we similarly construct salinity series for the coldest, deepest water overflowing the Denmark Strait sill (DS, freshening at −13 p.p.m. per decade, Fig. 2), for the fully entrained DSOW-derived water mass descending the Greenland slope in the western Irminger Sea (WIS DSOW, −15 p.p.m. per decade) and for the DSOW-derived water mass occupying the deepest layers of the Labrador Sea (LS DSOW, −12 p.p.m. per decade), we find an essentially similar trend and period of freshening.

Differences in detail between the freshening trends of the two overflows are understandable if we consider that the processes contributing to the freshening of the Nordic seas are uneven in distribution. For example, Fig. 2 shows an accelerated freshening at the Denmark Strait sill (DS), in the near-bottom overflow core off southeast Greenland (WIS DSOW) and in the abyssal Labrador Sea (LS DSOW) in the mid-1990s, followed by recovery to the common trend-line, which was not experienced in the NEADW layers close by (EIS NEADW and LS NEADW). We suggest that this reflects the peak 1–2 years earlier in the efflux of ice from the Fram Strait which would more directly affect the western overflow. To illustrate this, we superimpose in Fig. 2 an observed[17] ice-flux series (scale inverted).

Because both overflows are considerably altered by entrainment and mixing as they deepen and spread to the Labrador Sea[21], we might expect their freshening signal to dilute downstream, particularly along the 5,000-km path length of the eastern overflow.

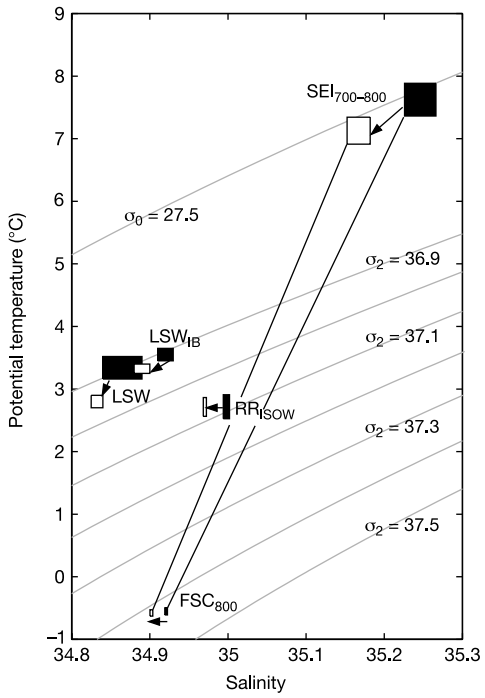

Figure 3 Maintenance of the freshening rate of Iceland-Scotland Overflow Water (ISOW) on its long spreading-path to the Labrador Sea. This freshening rate is maintained by the ISOW entraining or mixing with waters that are themselves freshening at an even greater rate. This potential temperature–salinity diagram describes the mixing relations in the South Iceland basin between overflow, entrainment and LSW, and takes account of the changing character of each of these three end-members between the 1960s (filled rectangles) and late 1990s (open rectangles). Lines of equal density, referenced adiabatically to the surface and to 2,000 dbar, are shown as σ_0 and σ_2, respectively. Cold, dense water crossing the sill of the Faroe–Shetland channel at 800 m depth (FSC_{800}) will initially entrain the warm salty resident water at around that depth as it passes westward along the Iceland–Faroe slope. That end–member ($SEI_{700–800}$) is assigned the characteristics of water at 700–800 m depth from immediately above the permanent thermocline in this region. The product of any simple mixing between these two water-types would fall on the line connecting them, so cannot explain the relative freshness of the ISOW core (RR_{ISOW}) encountered further south against the lower flanks of the Reykjanes Ridge. That freshening can only derive from mixing with a component of LSW, the freshest end-member shown. (Note that because data to describe the changing LSW-derivative in the south Icelandic basin are sparse, we show the locus of that modified LSW (LSW_{IB}), and that of LSW at source, the latter predated by 5 years.) The present analysis suggests that RR is formed in the proportions 43% FSC_{800}, 31% $SEI_{700-800}$, and 26% LSW_{IB}, although the recipe is approximate and can be expected to change with time.

So the maintenance of a more-or-less uniform freshening rate along that path (Fig. 2) is surprising. We identify two locations in particular where that freshening would be reinforced and so maintained.

The first concerns the entrainment and mixing that take place as the eastern overflow leaves the Faroe Bank channel at $>1\,m\,s^{-1}$ to descend and decelerate through the resident water masses at the head of the south Icelandic basin[22]. Selecting the 500–1,000 m layer immediately southeast of Iceland as representative of the entrained water masses, Fig. 2 indicates that its mean freshening rate was more than twice as large as that of the overflow itself (−32 p.p.m. per decade; SEI in Fig. 2). As Fig. 3 explains, however, we need three end-members—all of them freshening with time—to account for the changing ISOW characteristics at the base of the Reykjanes Ridge. Selecting the water that overflows the Faroe–Shetland channel at sill depth (800 m) as the 'source' end-member, and the warm saline water mass at 700–800 m south of Iceland as the likely initial 'entrainment' ($SEI_{700–800}$; Fig. 3), we find that we cannot form the product water mass that we encounter along the lower east side of the Reykjanes Ridge (RR_{ISOW}) or explain its freshening with time unless we add the cooling and freshening influence of a sizeable component of LSW. However, the freshening rate of LSW at source was also at least as large as that of the overflow (−13 p.p.m. per decade, 1965–2000, for LSW defined annually as the largest volumetric temperature–salinity class). Broadly speaking, Fig. 3 implies that the overflowing source water more than doubles in volume (about 2.5 ×) through entrainment and mixing along the margins of the south Icelandic basin, and that the other two end-members ($SEI_{700–800}$ and LSW) contribute about equally to the fully entrained product.

The divergence of curves EIS and WIS with time in Fig. 2 suggests that the NEADW layer undergoes further re-freshening in waters of the western Irminger Sea. Both curves show the salinity change on the isopycnal that lies at the core of the NEADW layer in the Irminger Sea ($\sigma_2 = 36.99–37.01$), but close to Greenland where this isopycnal shoals to 1,500–2,250 m, the freshening rate (WIS; −22 p.p.m. per decade) is much greater than in the centre of the basin (EIS, −13 p.p.m. per decade, depth range 2,120–2,550 m). We infer from this that NEADW entering from the eastern basin is re-freshened as it approaches, shoals and then passes south against the Greenland slope, either by mixing with the underlying DSOW layer, or the overlying LSW layer, or both. Thus salinities of WIS and EIS would be similar around 1970 when LSW formation was too shallow to influence that isopycnal, but diverge into the 1990s as deepening convection in the Labrador Sea carried colder and fresher LSW to a sufficient depth to influence NEADW properties in the western Irminger Sea.

We conclude then that the freshening rate of the eastern overflow was maintained downstream by mixing with waters that were themselves freshening at an equal or greater rate. A similar conclusion applies to the overflow from the Denmark Strait as it descends the Greenland slope to the abyssal Labrador Sea. As its volume rapidly doubles by entrainment south of the sill[21], its relatively uniform freshening rate is not simply the result of a short spreading-path but must reflect mixing with overlying waters of a similar or greater rate of freshening—LSW at −13 p.p.m. or WIS NEADW at −22 p.p.m. per decade.

We have described a widespread, sustained, rapid and surprisingly uniform freshening of the deep and abyssal North Atlantic, south of the Greenland–Scotland Ridge, over the past four decades. Because the freshening affects both overflows and their spreading pathways downstream, it seems to confirm our supposition that subarctic change can be rapidly transferred to the deep Atlantic, and has already directly affected the abyssal limb of the Atlantic meridional overturning circulation. Other observations confirm that the deep and abyssal freshening we describe has already passed equatorward along the North American seaboard in the Deep Western Boundary Current (W.M. Smethie, personal communication).

The question remains as to whether and to what extent these changes or these transfers reflect the onset of global change. With "new and stronger evidence"[3] of anthropogenic warming, coupled climate models seem to be reaching some kind of consensus that a slowdown of North Atlantic Deep Water production and of the meridional overturning circulation will be one outcome. However the issue of whether such effects are yet evident in our ocean time series remains open. Hansen *et al.*[4] have been able to couple a moderately long, modern set of direct flow measurements to a half-century of frequent hydrography at OWS M to provide evidence of a 20% decrease in the coldest and densest part ($T < 0.3\,°C$, $\sigma t > 28.0$, σ_t is *in situ* density) of the overflow from the Faroe Bank channel since 1950, and such measurements as we have from the Denmark Strait give no sign of any compensating increase in the cold dense outflow through that sill[23]. In the overflow hydrography that we report here, we provide the companion finding that a means exists of transferring the 'signal' of high-latitude climate change to the deep and abyssal headwaters of the global thermohaline circulation. However, the question of ultimate cause really hinges on whether the long amplification of the NAO, which so pervades our recent records of ocean circulation and hydrography, is itself attributable to global change; that issue is at present unresolved[12,24]. □

Received 15 October 2001; accepted 21 March 2002.

1. Rahmstorf, S. & Ganopolski, A. Long-term global warming scenarios computed with an efficient coupled climate model. *Clim. Change* **43,** 353–367 (1999).
2. Delworth, T. L. & Dixon, K. W. Implications of the recent trend in the Arctic/North Atlantic Oscillation for the North Atlantic thermohaline circulation. *J. Clim.* **13,** 3721–3727 (2000).
3. IPCC *Climate Change 2001: The Scientific Basis* (eds Houghton, J. T. *et al.*) (Cambridge Univ. Press, Cambridge, 2001).
4. Hansen, B., Turrell, W. R. & Østerhus, S. Decreasing overflow from the Nordic seas into the Atlantic Ocean through the Faroe-Shetland Channel since 1950. *Nature* **411,** 927–930 (2001).
5. Curry, R. & McCartney, M. S. Ocean gyre circulation changes associated with the North Atlantic Oscillation. *J. Phys. Oceanogr.* **31,** 3374–3400 (2001).
6. Lazier, J. R. N. in *Natural Climate Variability on Decade-to-Century Time Scales* (eds Martinson, D. G. *et al.*) 295–304 (National Academy Press, Washington DC, 1995).
7. Verduin, J. & Quadfasel, D. in *European Sub-Polar Ocean Programme II, Final Scientific Report* (ed. Jansen, E.) A1, 1–11 (Univ. Bergen, Bergen, 1999).
8. Lascaratos, A., Roether, W., Nittis, K. & Klein, B. Recent changes in deep water formation and spreading in the eastern Mediterranean Sea. *Prog. Oceanogr.* **44,** 5–36 (1999).
9. Gordon, A. Weddell Deep Water variability. *J. Mar. Res.* **40,** 199–217 (1982).
10. Hurrell, J. W. Decadal trends in the North Atlantic Oscillation: regional temperatures and precipitation. *Science* **269,** 676–679 (1995).
11. Dickson, R. R., Lazier, J., Meincke, J., Rhines, P. & Swift, J. Long-term co-ordinated changes in the convective activity of the North Atlantic. *Prog. Oceanogr.* **38,** 241–295 (1996).
12. Hurrell, J. W. & Dickson, R. R. in *Ecological Effects of Climate Variations in the North Atlantic* (eds Stenseth, N. C., Ottersen, G., Hurrell, J. W. & Belgrano, A.) (Oxford Univ. Press, in the press).
13. Sy, A. *et al.* Surprisingly rapid spreading of newly formed intermediate waters across the North Atlantic Ocean. *Nature* **386,** 675–679 (1997).
14. Brewer, P. G. *et al.* A climatic freshening of the deep Atlantic north of 50°N over the past 20 years. *Science* **222,** 1237–1239 (1983).
15. Swift, J. H. *Climate Processes and Climate Sensitivity* (eds Hansen, J. E. & Takehashi, T.) 39–47 (AGU Geophysical Monograph 29, American Geophysical Union, Washington DC, 1984).
16. Vinje, T., Nordlund, N. & Kvambekk, A. Monitoring ice thickness in Fram Strait. *J. Geophys. Res.* **103,** 10437–10449 (1998).
17. Vinje, T. Fram Strait ice fluxes and atmospheric circulation, 1950-2000. *J. Clim.* **14,** 3508–3517 (2001).
18. Dickson, R. R. *et al.* The Arctic Ocean response to the North Atlantic Oscillation. *J. Clim.* **13,** 2671–2696 (2000).
19. Blindheim, J. *et al.* Upper layer cooling and freshening in the Norwegian Sea in relation to atmospheric forcing. *Deep-Sea Res. I* **47,** 655–680 (2000).
20. Turrell, W. R., Slesser, G., Adams, R. D., Payne, R. & Gillibrand, P. A. Decadal variability in the composition of Faroe-Shetland Channel bottom water. *Deep-Sea Res. I* **46,** 1–25 (1999).
21. Dickson, R. R. & Brown, J. The production of North Atlantic Deep Water: Sources, rates and pathways. *J. Geophys. Res. C* **99,** 12319–12341 (1994).
22. Hansen, B. & Østerhus, S. North Atlantic–Nordic seas exchanges. *Prog. Oceanogr.* **45,** 109–208 (2000).
23. Girton, J. B., Sanford, T. B. & Käse, R. H. Synoptic sections of the Denmark Strait Overflow. *Geophys. Res. Lett.* **28,** 1619–1622 (2001).
24. Thompson, D. W. J., Wallace, J. M. & Hegerl, G. C. Annular modes in the extratropical circulation Part II: Trends. *J. Clim.* **13,** 1018–1036 (2000).

Acknowledgements

We thank S.-A. Malmberg and H. Valdimarsson for the use of unpublished hydro-data from the Icelandic Standard Sections Programme, and A. Clarke and J. Lazier, whose efforts provided much of the Labrador Sea data that we use here. This work was part of the data synthesis phase of the WOCE Program, of the VEINS Project of the MAST III

Programme of the European Community, and of the NOAA Consortium on the Ocean's Role in Climate of Scripps Institution of Oceanography, San Diego and Lamont-Doherty Earth Observatory, Palisades, New York; it was supported in part by the Office of Polar Programs and Geosciences Directorate of the NSF.

Competing interests statement

The authors declare that they have no competing financial interests.

Correspondence and requests for materials should be addressed to R.R.D. (e-mail: r.r.dickson@cefas.co.uk).

Ecosystem consequences of species richness and composition in pond food webs

Amy L. Downing* **& Mathew A. Leibold**

Department of Ecology and Evolution, University of Chicago, 1101 E. 57th Street, Chicago, Illinois 60637, USA

Resolving current concerns about the role of biodiversity on ecosystems calls for understanding the separate roles of changes in species numbers and of composition. Recent work shows that primary productivity often, but not always, saturates with species richness within single trophic levels[1–8]. However, any interpretation of such patterns must consider that variation in biodiversity is necessarily associated with changes in species composition (identity)[9–12], and that changes in biodiversity often occur across multiple trophic levels[13,14]. Here we present results from a mesocosm experiment in which we independently manipulated species richness and species composition across multiple trophic levels in pond food webs. In contrast to previous studies that focused on single trophic levels, we found that productivity is either idiosyncratic or increases with respect to species richness, and that richness influences trophic structure. However, the composition of species within richness levels can have equally or more marked effects on ecosystems than average effects of richness *per se*. Indirect evidence suggests that richness and associated changes in species composition affect ecosystem attributes through indirect effects and trophic interactions among species, features that are highly characteristic of natural, complex ecosystems.

The role of biodiversity in ecosystems is important both because it can reveal basic insights into the functioning of ecosystems, and because it has implications for how humans respond to current losses in global biodiversity. In a given situation, changes in biodiversity will influence local ecosystems depending on the identity[5,15–18] and number[4,6,8,18,19] of species going extinct. The effects of biodiversity on ecosystems may also depend on whether declines in biodiversity occur at a single trophic level compared with multiple trophic levels[13] when ecosystem processes are influenced by the complex set of species and trophic interactions in communities[1,20]. Here we ask how changes in species composition and richness affect ecosystems when they occur across multiple trophic levels. We focus our analysis on ecosystem attributes that indicate the importance of indirect effects of species in ecosystems.

We tested the effects of species composition and species richness in selected trophic functional groups of pond communities—macrophytes, benthic (bottom-dwelling) grazers and carnivorous predators—while holding functional group diversity constant in field mesocosms. These functional groups were chosen because they are dominant functional groups in fishless ponds, they represent three different trophic levels, and they can be experimentally manipulated with little threat of contamination. The mesocosms also contained decomposers, phytoplankton, periphyton and zooplankton, which together with the manipulated functional groups account for the dominant functional groups in aquatic systems[21]. Although natural ponds differ from the mesocosms in some respects, the mesocosms were subject to natural fluctuations in light, temperature and rainfall, and should represent better analogues of natural systems than more controlled laboratory situations.

The experiment was designed to examine the impacts of declining richness while simultaneously estimating the relative impact of random compositional changes that are associated with biodiversity loss. To disentangle effects of richness from composition, we nested species composition treatments within diversity treatments (see Methods for details). First, we created three species richness treatments with one, three or five species per functional group. Second, within each level of richness, we nested and replicated seven unique species compositions (particular combinations of species). Testing for the effects of all possible combinations is experimentally prohibitive; however, we tested for the effects of seven random draws of species compositions from a fixed species pool within each richness level, providing an unbiased sample of possible species combinations. To draw attention to the effects of composition *per se* rather than the effects of extinction-prone species, we treat all manipulated species equally. Thus our approach does not consider how likely each of the manipulated species is to go extinct, and we emphasize that in situations of environmental concern, compositional effects will depend on additional factors that determine which species are most likely to go extinct[13,22]. We also recognize that as a greater number of species are lost from a community, the number of possible species combinations changes and the proportional similarities between combinations may decrease.

We monitored ecosystem attributes other than the manipulated species in order to capture the importance of trophic interactions and indirect effects of the manipulated species in ecosystems. Specifically, we measured decomposition rates, and phytoplankton, periphyton and zooplankton biomass, all of which are primarily measures of the activities or abundances of unmanipulated functional groups. For example, predators consume zooplankton and benthic grazers. Zooplankton and benthic grazers in turn consume phytoplankton, periphyton, and decomposers. The ecosystem response variables also included ecosystem productivity and respiration, as calculated from diurnal oxygen cycles[23]. In our system, ecosystem productivity and respiration are determined primarily by periphyton, phytoplankton and microbes (based on allometric calculations involving the metabolism and biomass of these organisms), providing a broad measure of collective metabolic activity in the larger community primarily involving trophic groups that were not manipulated.

Our results show that ecosystem productivity is greatest at the highest richness level (Fig. 1b and Table 1). Treatments with three and nine species had very similar and slower rates compared with the most diverse communities of 15 species. Unlike previous studies, we found that effects of species richness on productivity and respiration did not saturate and were synergistic[3], enhanced in only the most diverse communities, at least over this range of richness levels. Patterns for respiration are similar but not quite significant (Fig. 1c and Table 1). Richness also influences the partitioning of plankton biomass within the ecosystems (Fig. 1d–f and Table 1). Phytoplankton biomass increased and zooplankton and periphyton biomass decreased with richness. In contrast, species richness did not significantly alter the total biomass of any of the manipulated functional groups (macrophytes, $F = 0.15$,

* Present address: Department of Zoology, Ohio Wesleyan University, Delaware, Ohio 43015, USA.